Absolute and Convective Instabilities of a Viscous Film Flowing Down a Vertical Fiber

C. Duprat,[1] C. Ruyer-Quil,[1] S. Kalliadasis,[2] and F. Giorgiutti-Dauphiné[1]

[1]*CNRS, Univ Pierre et Marie Curie, Univ Paris-Sud, Lab FAST, Bat 502, Campus Univ, Orsay 91405, France*

[2]*Department of Chemical Engineering, Imperial College London, London SW7 2AZ, United Kingdom*

(Received 14 December 2006; published 15 June 2007)

The stability of a viscous film flowing down a vertical fiber under the action of gravity is analyzed both experimentally and theoretically. At large or small film thicknesses, the instability is convective, whereas an absolute instability mode is observed in an intermediate range of film thicknesses for fibers of small enough radius. The onset of the experimental irregular wavy regime corresponds precisely to the theoretical prediction of the threshold of the convective instability.

DOI: 10.1103/PhysRevLett.98.244502 PACS numbers: 47.20.Ma, 68.03.Kn, 68.15.+e

The general problem of instability and pattern formation involving propagating modes has attracted much theoretical and experimental interest (see, e.g., [1]). Instabilities can be either *convective* (disturbances grow in time only in a moving frame) or *absolute* (disturbances grow in time even at a fixed position). This concept was first developed in the context of plasma physics [2] and later on applied to optics and hydrodynamics [3].

In particular, transitions between different wave regimes in open-flow hydrodynamic systems can be understood within the framework of absolute or convective instabilities. Convectively unstable flows behave as spatial amplifiers of the incoming perturbations, whereas absolutely unstable flows display intrinsic self-sustained dynamics or *global modes*. The transition between these two classes of flows has been experimentally evidenced in numerous situations, e.g., wakes or hot jets [4].

Viscous liquid films falling down inclined planes are an example of convectively unstable open flows [5,6]. On the other hand, changing the geometry from planar to cylindrical, such as with free jets, can make the flow absolutely unstable [7]. In this Letter, we demonstrate for the first time that a thin viscous layer, coating the outside of a vertical cylinder, and flowing under the action of gravity can also display both convective and absolute instabilities.

While the dynamics of the flow on a cylinder has received considerable attention over the last two decades (see, e.g., [8] for a review), all previous works focused either on a temporal stability analysis or the fully nonlinear wave regime [9–12]. Here we examine in detail, both experimentally and theoretically, the onset of instability with an emphasis on its spatial growth. Unlike jets where the absolute instability breaks the flow into drops, in the present case the flow is always continuous. At the same time, the Reynolds number is much smaller than for jets, which makes the problem amenable to theoretical analysis. Moreover, since the base flow is strictly parallel, a situation that is quite exceptional (e.g., jets in microgravity or sheared interfaces in confined geometries [13]), this problem offers an excellent opportunity to study experimentally the development of nonlinear global modes [4]. The experiments can achieve a wide range of flow rates and in a certain regime of the parameter space the flow can be controlled relatively easily.

A sketch of the experimental setup is shown in Fig. 1(a). A Rhodorsil silicon oil v50 (density $\rho = 963$ kg/m^3, kinematic viscosity $\nu = 50 \times 10^{-6}$ m^2/s and surface tension $\gamma = 20.8 \times 10^{-3}$ N/m at 25 °C) flows axisymmetrically on Nylon fibers of 1.35 m length and of various radii R (0.23, 0.25, 0.32, 0.35, 0.47 and 1.5 mm). A weight tied to the fiber ensures its verticality. The inlet flow rate q is controlled by varying the gap separating the two cone-shaped parts of the entrance valve. This design ensures the axisymmetry of the base flow and limits the entrance noise (thickness fluctuations of 10^{-3}%; estimation based on the computation of the maximum spatial growth rate in the convective regime). The possible range of flow rates is 0.01 g/s $< q < 3$ g/s, which corresponds to a range of

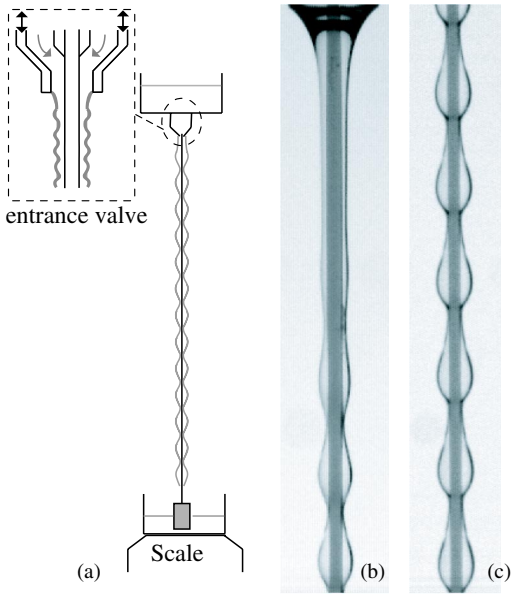

FIG. 1 (color online). (a) Experimental setup. (b) and (c) Snapshots of the liquid film at the top of the fiber and at 10 cm from the entrance valve, respectively, showing a nonlinear regular wave train ($R = 0.23$ mm, $q = 0.0348$ g/s and $h_N = 0.48$ mm).

 © 2007 The American Physical Society

uniform film thicknesses $0.6R < h_N < 3R$ (corresponding values of dimensionless parameters will be given later). The flow rate is measured with computer-controlled scales placed below the collecting tank. During an experiment, the liquid height variation in the tank (hence the flow rate variation) is less than 1%. A linear camera and a fast digital camera are mounted on micrometric assemblies allowing for a precise alignment of the field of view with the film for the linear camera and a precise displacement along the fiber for the fast one. Spatiotemporal diagrams obtained with the linear camera (using a vertical pixel line) allow for a sensitive detection of the film-thickness variations. Fluctuations of the film thickness with time at a given position are also recorded by orienting horizontally the pixel line.

A snapshot of the flow at the inlet is depicted in Fig. 1(b) for a small flow rate on a thin fiber. A self-sustained dynamics is observed. Immediately after the inlet, the axisymmetric film of uniform thickness emerging from the capillary meniscus breaks up spontaneously into a droplike wave train. Depending on the flow rate and the fiber radius, two different regimes can be identified from the spatiotemporal evolution of the film thickness (see Fig. 2). At low flow rates and relatively small fiber radii, a regular primary wave train is observed at a constant distance from the inlet. Sufficiently close to the inlet, a power spectrum of the time variations of the film thickness reveals a well-defined frequency. Further downstream, a secondary instability disorganizes the flow. However, for even smaller fiber radii and over a rather narrow interval of (small) flow rates (the thinner the fiber the wider the range of flow rates), the waves propagate at constant speed, shape, and frequency all along the fiber [see Fig. 1(c)]. This global mode regime was observed initially by Kliakhandler *et al.* [9]. At larger flow rates and any radius, the primary wave train is irregular, its frequency spectrum is much broader and its onset location fluctuates in time. For thick fibers ($R \geq 0.47$ mm) the regular wave regime was never observed.

A quantity of particular interest is "the healing length" Δ defined as the distance from the inlet to the location at which perturbations on the film are noticeable (>4% of the uniform film thickness). The evolutions of Δ and frequency f with the flow rate for $R = 0.32$ mm are shown in Fig. 3. Bars indicate the extreme values of Δ and f. The transition between regular and irregular wavy regimes can be clearly identified at a critical flow rate $0.042 < q_c < 0.048$ g/s as a sharp increase of the possible range of values for both Δ and f. We shall not address here the question of the secondary stability of the self-sustained nonlinear primary oscillations in the global mode regime [compare Fig. 1(b) and 2], but limit ourselves to the linear convective stability of the constant thickness base flow in an attempt to understand the transition between regular and irregular wave trains.

Assuming negligible inertia and a small thickness h compared to R, Frenkel [10] obtained the following evolution equation:

$$\partial_t h + \partial_x\left[\frac{h^3}{3}(1 + \beta\partial_x h + \partial_{x^3} h)\right] = 0. \qquad (1)$$

Here the streamwise coordinate x and h have been made dimensionless using different length scales, $\mathcal{L} = \kappa h_N$ and h_N, where h_N is the flat film thickness and κ is adjusted such that the gravity acceleration ρg equilibrates the pressure gradient induced by the axial curvature gradient $\gamma\partial_{x^3} h$. Thus, $\kappa = [\gamma/(\rho g h_N^2)]^{1/3} = (l_c/h_N)^{2/3}$, where l_c is the capillary length. The chosen time scale $\mathcal{T} = \kappa h_N/(3u_N)$ is one third of the advection time, where $u_N = gh_N^2/(3\nu)$ is the averaged speed of a film flowing down a vertical wall. With this scaling, Eq. (1) involves a unique positive parameter $\beta = (\mathcal{L}/R)^2$ that expresses the relative importance of azimuthal and axial curvatures [Kalliadasis and Chang [11]; the same study also scrutinized the nonlinear solutions of (1)].

A normal mode decomposition of infinitesimal perturbations around the uniform film $h = 1$ in (1) leads to the dispersion relation

$$\omega = k + \frac{ik^2}{3}(\beta - k^2), \qquad (2)$$

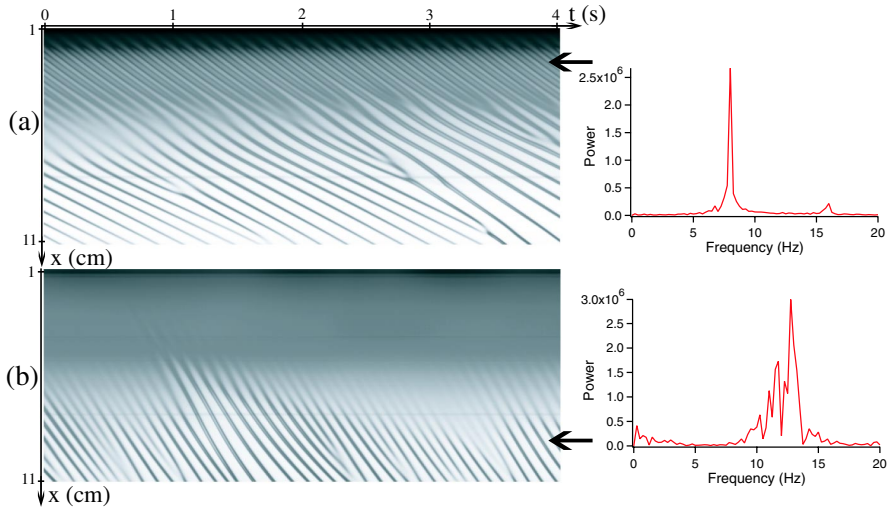

FIG. 2 (color online). Left: spatiotemporal diagrams of the film thickness along the fiber. x is the distance from the top of the fiber. Right: power spectra. The locations at which the time series have been recorded are indicated by arrows. $R = 0.32$ mm; (a) $q = 0.024$ g/s ($h_N = 0.42$ mm); (b) $q = 0.077$ g/s ($h_N = 0.58$ mm).

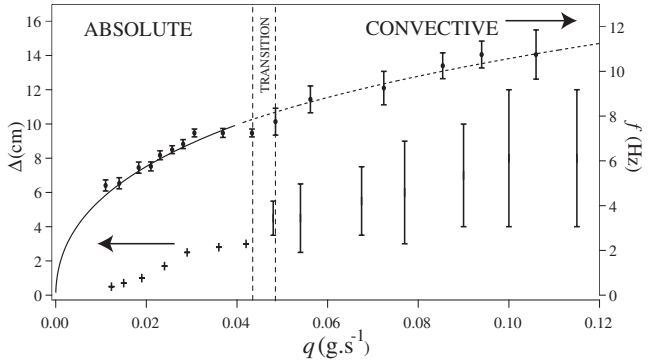

FIG. 3. Healing length (left ordinate) and frequency (right ordinate) versus flow rate at $R = 0.32$ mm. Solid and dashed lines correspond to the absolute frequency and the frequency of the maximum spatial growth rate, respectively. Both are obtained from the OS analysis.

where k and ω denote the complex wave number and complex wave frequency, respectively. Hence, perturbations of long wavelengths and of infinite spatial extension (k real) are simply advected at the kinematic wave velocity of unity. The linear inception is driven by the classical Rayleigh-Plateau instability for cylindrical interfaces. Hence, short waves are damped by the axial curvature and long waves are amplified by the azimuthal curvature.

The long-time response of the flow to a localized infinitesimal perturbation at a fixed location is determined by the most amplified wave of zero group velocity $v_g = d\omega/dk$, which defines the absolute wave pulsation ω_0 and absolute wave number k_0. Looking for the spatial branches $k(\omega)$ (imaginary part $\omega_i = cst$) in the complex k plane, the condition $v_g = 0$ occurs at a saddle point that must result from the pinching of two spatial branches coming from the opposite side of the horizontal axis [3]. A straightforward analysis based on (2) then shows that the instability becomes absolute ($\omega_{0i} > 0$) when $\beta > \beta_{ca} \equiv [(9/4)(-17 + 7\sqrt{7})]^{1/3} \approx 1.507$. With $\beta = \alpha_N^{2/3}(l_c/R)^{4/3}$, where $\alpha_N = h_N/R$, an aspect ratio, $\beta > \beta_{ca}$ reads

$$\alpha_N > \beta_{ca}^{3/2}(R/l_c)^2. \tag{3}$$

A localized disturbance may therefore invade the spatial domain whenever the Rayleigh-Plateau instability is stronger than the advection of the main flow, as reflected by the threshold β_{ca}. It is quite remarkable that the threshold β_{ca} of the transition from a convective to an absolute instability (C/A transition) is close to the value $\beta_c \approx 1.413$ above which a catastrophic growth of the speed and amplitude of the nonlinear solitary-wave solutions to (1) occurs as shown by Kalliadasis and Chang [11]. In their study the unbounded growth observed for $\beta \gtrsim 1.413$ was associated with the drop formation process first observed experimentally by Quéré [8] (the last stage of the nonlinear evolution for sufficiently thin films). However, the ultimate details of this process cannot be captured by (1) as the assumption of a thin film thickness h in comparison to the fiber radius R is soon violated when the drops reach a size typically of the order of R. This assumption was relaxed in the study by Kliakhandler, Davis, and Bankoff [9] (KDB) who obtained the following equation (referred to hereafter as KDB)

$$\partial_t\left(h + \frac{\alpha_N}{2}h^2\right) + \partial_x\left\{\frac{h^3}{3}\frac{\phi(\alpha_N h)}{\phi(\alpha_N)}[1 + \partial_x K(h)]\right\} = 0, \tag{4}$$

where $\phi(\alpha) = [3(4(\alpha+1)^4\log(\alpha+1) - \alpha(\alpha+2)\times(3\alpha(\alpha+2)+2))]/(16\alpha^3)$ is a geometric factor corresponding to the flow rate per unit length

$$q_N = g h_N^3 \phi(\alpha_N)/(3\nu) \tag{5}$$

for a uniform film of thickness h_N, and $K(h)$ is the full mean free-surface curvature. Craster and Matar [12] derived an evolution equation nearly identical to the KDB model in (4), the only difference being the estimation $\partial_{x^2} h$ for the axial curvature. Equation (4) is nondimensionalized using a modified time scale $\mathcal{T}' = \mathcal{T}/\phi(\alpha_N)$ such that $h = 1$ still corresponds to a flow rate $q = 1/3$.

A linear stability analysis of both the KDB and Craster-Matar equations leads to the same dispersion relation

$$\omega = k c_k(\alpha_N) + \frac{ik^2}{3(1+\alpha_N)}\left(\frac{\beta}{(1+\alpha_N)^2} - k^2\right), \tag{6}$$

where $c_k = \{1 + \alpha_N\phi'(\alpha_N)/[3\phi(\alpha_N)]\}/(1+\alpha_N)$ is the speed of the linear kinematic waves of (6) for $k \to 0$. Equation (2) can be recovered from (6) through the transformation $k \to k[c_k(1+\alpha_N)]^{1/3}$, $\omega \to \omega c_k^{4/3}(1+\alpha_N)^{1/3}$ and $\beta \to \beta c_k^{2/3}(1+\alpha_N)^{8/3}$. As a consequence, the threshold above which the instability governed by the dispersion

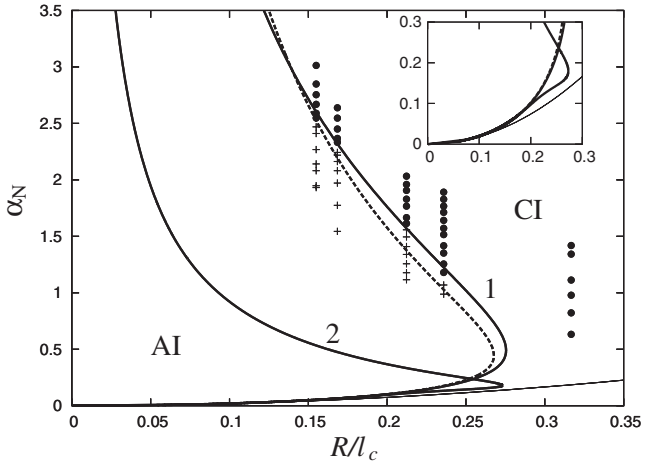

FIG. 4. AI and CI regions in the parameter plane $\alpha_N = h_N/R$ versus R/l_c. Thick solid lines refer to the OS solutions; label 1 refers to Rhodorsil silicon oil v50 and label 2 to water. Dashed and thin solid lines correspond to Eqs. (7) and (3), respectively. Regular and irregular primary wave trains reported in the experiment are indicated by crosses and dots, respectively. The dependence of h_N (and thus α_N) with the flow rate q_N is given in (5). The inset is a blowup of the diagram for small values of α_N.

relation (6) becomes absolute can be readily obtained from the analysis of (2). The C/A transition then occurs at

$$\frac{\alpha_N}{c_k(\alpha_N)(1+\alpha_N)^4} > \beta_{ca}^{3/2}\left(\frac{R}{l_c}\right)^2. \quad (7)$$

In Fig. 4 we compare the boundary between convective instability (CI) and absolute instability (AI) regions given by (3) and (7) to the one obtained from the linear stability analysis of the axisymmetric Navier-Stokes equations. The resulting Orr-Sommerfeld (OS) equation, a fourth-order ordinary differential equation for the complex streamfunction $\psi(r)$ with r the radial coordinate and completed with the linearized stress balance and the no-slip condition at the fiber, was solved numerically by continuation starting from the planar limit ($R \to \infty$) and a very thin film (Reynolds number $Re \to 0$) in which case the solutions to the OS equation can be obtained analytically.

The limit of small film thicknesses compared to the fiber radius, $\alpha_N \to 0$, corresponds to the case of a film flowing down a vertical wall for which the instability is always convective [5]. In the case of thick films, i.e. α_N large, the Rayleigh-Plateau instability is weakened by the decrease of the free-surface azimuthal curvature, $1/(R + h_N)$. This effect is not compensated by the lower speed of the kinematic waves relative to the mean flow as α_N increases, and the instability is again convective. As a consequence, at a given value of the radius R, there exists an intermediate range of α_N values for which the Rayleigh-Plateau mechanism dominates over the advection of the waves, the instability being therefore absolute. On the other hand, the instability is always convective for fibers of larger radii, i.e. $R > 0.28 l_c$. Interestingly, this latter value seems to be independent of the liquid viscosity. For highly viscous liquids, such as Rhodorsil silicon oil v50, the locus of the C/A transition (thick line labeled 1 in Fig. 4) is close to the zero-inertia limit (7).

Figure 4 summarizes the experimental findings for different fiber radii. Primary sinusoidal wave trains of constant frequencies and healing lengths are reported as crosses. Wave trains displaying significant fluctuations of the frequency or the healing length are indicated by dots. The transition between both regimes is in good agreement with the C/A boundary (curve 1). In the AI region, the frequency of the primary waves corresponds to the frequency of the linear absolute mode (see Fig. 3). Therefore we conclude that the onset of the regular wavy regime coincides precisely with the onset of the absolute instability.

The effects of inertia can be observed for less viscous fluids, like water ($\nu = 10^{-6}$ m^2/s and $\gamma = 72.5 \times 10^{-3}$ N/m). The OS analysis reveals a C/A boundary in parameter space (curve 2 in Fig. 4) topologically similar to what is found with the zero-inertia approximation of the KDB model in (4). Yet, significant deviations from (7) are observed at small values of α_N, inertia tends to enlarge the AI region as it reinforces the destabilizing azimuthal curvature that competes with advection. However, at large values of α_N, corresponding to large Reynolds numbers, the classical hydrodynamic instability of a falling film dominates over the Rayleigh-Plateau mechanism. Consequently, the characteristics of the instability in this region are similar to the vertical planar case where the instability is always convective [5].

To conclude, we have characterized experimentally and theoretically the primary instability of a viscous film flowing down a fiber. Evidence of both regular and irregular wavy regimes has been obtained through measurements of the healing length and frequency of the signal close to the inlet. A convective stability analysis, based on the approximate zero-inertia evolution Eqs. (1) and (4), as well as the linearized primitive equations, has been undertaken. The threshold of the regular wavy regime is shown to correspond precisely to the linear C/A transition, as suggested by the Ginzburg-Landau formulation for a supercritical Hopf bifurcation [4]. The critical flow rate for the CI onset is in good agreement with the experimental transition from regular to irregular primary wave trains for all tested fiber radii. Of particular interest would be the structure and the stability of the observed global mode. At the same time, for large α_N where the dynamics is driven by both the hydrodynamic mode of instability for a film on planar substrate and the Rayleigh-Plateau instability, we anticipate that the coupling between the two can lead to some intricate nontrivial wave dynamics in the nonlinear regime. We shall examine these and related issues in a future study.

We thank P. Jenffer and G. Marteau for technical assistance, and J. P. Hulin, T. Loiseleux, M. Rossi, and M. Rabaud for warm and fruitful discussions. S. K. thanks Lab. FAST for hospitality and financial support.

[1] *Propagation in Systems Far from Equilibrium*, edited by J. E. Wesfreid, H. R. Brand, P. Manneville, G. Albinet, and N. Boccara (Springer-Verlag, Berlin, 1988).
[2] R. J. Briggs, *Electron-Stream Interaction with Plasmas* (MIT, Cambridge, MA, 1964).
[3] P. Huerre and P. A. Monkewitz, Annu. Rev. Fluid Mech. **22**, 473 (1990).
[4] J.-M. Chomaz, Annu. Rev. Fluid Mech. **37**, 357 (2005).
[5] L. Brevdo, F. Dias, T. J. Bridges, and P. Laure, J. Fluid Mech. **396**, 37 (1999).
[6] H.-C. Chang and E. A. Demekhin, *Complex Wave Dynamics on Thin Films* (Elsevier, Amsterdam, 2002).
[7] S. J. Leib and M. E. Goldstein, J. Fluid Mech. **168**, 479 (1986).
[8] D. Quéré, Annu. Rev. Fluid Mech. **31**, 347 (1999).
[9] I. L. Kliakhandler, S. H. Davis, and S. G. Bankoff, J. Fluid Mech. **429**, 381 (2001).
[10] A. L. Frenkel, Europhys. Lett. **18**, 583 (1992).
[11] S. Kalliadasis and H.-C. Chang, J. Fluid Mech. **261**, 135 (1994).
[12] R. V. Craster and O. K. Matar, J. Fluid Mech. **553**, 85 (2006).
[13] P. Gondret, P. Ern, L. Meignin, and M. Rabaud, Phys. Rev. Lett. **82**, 1442 (1999).